CORE
Metadata, citation and similar papers at core.ac.uk
Provided by CERN Document Server

PHYSICAL REVIEW D **69**, 032001 (2004)

Landau-Pomeranchuk-Migdal effect for multihundred GeV electrons

H. D. Hansen and U. I. Uggerhøj
Department of Physics and Astronomy, University of Aarhus, Denmark

C. Biino
CERN, Geneva, Switzerland

S. Ballestrero, A. Mangiarotti, and P. Sona
University of Florence, Florence, Italy

T. J. Ketel
Free University, Amsterdam, The Netherlands

Z. Z. Vilakazi
University of Cape Town, Cape Town, South Africa
(Received 30 September 2003; published 13 February 2004)

Experimental results for the bremsstrahlung energy loss of 149, 207, and 287 GeV electrons in thin Ir, Ta, and Cu targets are presented. For each target and energy, a comparison between simulated values based on the Landau-Pomeranchuk-Migdal (LPM) suppression of incoherent bremsstrahlung is shown. For the electron energies investigated, the LPM effect enters the quantum regime where the recoil imposed on the electron by the emitted photon becomes important. Good agreement between simulations based on Migdal's theory and data from the experiment is found, indicating that the LPM suppression is well understood also in the quantum regime. Results from a comparison between simulations with the ''threshold'' energy E_{LPM} as a free parameter and the data are shown. This analysis reproduces the expected trend as a function of nominal radiation length, but yields values that tend to be low compared to Migdal's theory.

DOI: 10.1103/PhysRevD.69.032001 PACS number(s): 41.60.−m, 07.85.Fv, 29.40.Vj, 95.30.Gv

I. INTRODUCTION

This paper is a sequel to a previous publication [1] in which the increase of the effective radiation length as a result of the Landau-Pomeranchuk-Migdal (LPM) effect [2,3] is reported. We now present an experimental evaluation of the decisive parameter for the LPM effect, the ''threshold'' energy E_{LPM}. Furthermore, we supplement our previous publication in giving more details on the experiment, the analysis, as well as in presenting the full data set comprising Ir, Ta and Cu, each for three energies. Thus, a systematic analysis of E_{LPM} as a function of the nominal radiation length X_0 and the photon emission as a function of electron energy E can be performed.

The LPM effect is important in a variety of contexts. It has a significant impact on the behavior of air showers in the neighborhood of the Greisen-Zatsepin-Kuz'min cutoff of high energy photons [4–7], especially on the composition of the shower [8–10]. Moreover, the LPM effect in QED processes has a parallel in the suppression of gluons in QCD processes [11–17] and even neutrino radiation from cores of supernovae [18]. Finally, an electromagnetic shower initiated by an energetic electron in an electromagnetic calorimeter may develop over a characteristic length that is increased substantially compared to the nominal radiation length.

Several previous experiments have presented evidence for the LPM effect, see e.g., [19]. However, only the SLAC experiment performed with 8 and 25 GeV electrons [20–22] can be considered a truly successful systematic study of the effect in amorphous targets. This experimental study spurred a lot of theoretical interest e.g., to increase the accuracy of calculations [23–29] and to consider so-called ''structured targets'' [28,30,31], calculations of Delbrück scattering [32], evaluations of photon emission from quark-gluon plasmas [33,34] and reformulations of the QED case for subsequent use in QCD [35–38]. Several groups have calculated the LPM effect by means of different methods. In [19] a comprehensive review can be found and in order not to be too repetitive, the present paper to a large extent refers to work more recent than [19].

The motivation of the present investigation is to extend the energy regime of accelerator-based experimental studies of the LPM effect. In particular the aim is to verify the increase of the effective radiation length and examine the validity of the theory for bremsstrahlung photon energies comparable to the energy of the electron—the quantum regime.

II. THEORY

A. Formation length

Surprising to many, even to Landau [39], it takes a relatively long time and therefore a long distance for an energetic electron to create a photon. The interactions of the electron over this ''formation zone'' affect the radiation spectrum decisively and may lead to enhancement (as in the case of crystals, see e.g., [40]) or reduction of total intensity as well as changes in the spectral shape.

 ©2004 The American Physical Society

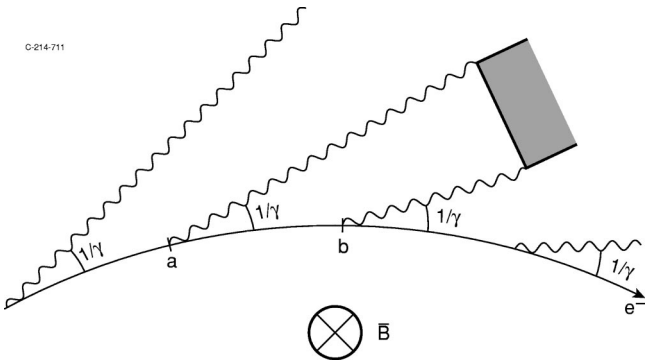

FIG. 1. Synchrotron radiation emission by an energetic electron traversing a magnetic field, *B*. The typical emission angle, $1/\gamma$, makes photon emission from any point within the arc length from *a* to *b* indistinguishable. Therefore, the distance *ab* represents the formation length.

1. Classical formation length

It is illustrative to consider a couple of approaches to the formation length as it appears in a classical theory. One approach is to consider the photon ''formed'' by the time it takes for a photon to advance with respect to the electron by one reduced wavelength, $\lambda/2\pi$ and by the corresponding distance of travel of the electron, l_{f},

$$\frac{l_{\mathrm{f}}}{v}=\left(l_{\mathrm{f}}+\frac{\lambda}{2\pi}\right)\frac{1}{c} \tag{1}$$

which for $v=(1-1/\gamma^2)c\simeq c$ yields

$$l_{\mathrm{f}}=\frac{2\gamma^2 c}{\omega} \tag{2}$$

where v is the speed of the electron, c the speed of light and $\gamma=E/mc^2$ the Lorentz factor related to the energy of the electron, E, and its rest mass, m. This is also one way to consider the formation length in QCD [13].

Another, more experimentally inclined approach, is to consider the emission of synchrotron radiation in a bending magnet with a field B as e.g., in a synchrotron light source. The typical emission angle of photons is $1/\gamma$—a result of the relativistic transformation. Thus, a detector unable to resolve angles smaller than $1/\gamma$ will yield no information on the actual position of radiation emission over the formation length, *a* to *b*, see Fig. 1. Since the emission angle, $1/\gamma$, connects the curvature radius, $r=pc/eB$, and the formation length, l_{f}, by $l_{\mathrm{f}}=r/\gamma$ for small angles, the result is

$$l_{\mathrm{f}}=\frac{pc}{eB\gamma} \tag{3}$$

and since synchrotron radiation has a ''characteristic'' frequency $\omega_c=3\gamma^3 eB/2p$, Eq. (2) is obtained again, although with a slightly different constant which depends on the choice of characteristic frequency.

2. Quantum formation length

In the quantum version, where e.g., recoil is taken into account, the formation length is given for emission of radiation as [41]

$$l_{\mathrm{f}}=\frac{2\gamma^2 c}{\omega^*} \quad \text{with} \quad \omega^*=\omega\cdot\frac{E}{E-\hbar\omega}\simeq\omega \tag{4}$$

where $\hbar\omega$ is the energy of the photon, [41]. The quantum formation length is calculated by use of the minimum longitudinal momentum transfer to the nucleus, $q_{\parallel}=p_i-p_f-\hbar\omega/c$ and using the uncertainty relation $l_f=\hbar/q_{\parallel}$ where p_i and p_f denote the momentum of the electron before and after the radiation event, respectively. Alternatively, Eq. (4) can be derived from arguments similar to those leading to Eq. (3) simply by taking the recoil into account [42]. In the classical or recoil-less limit, $\hbar\omega\ll E$, Eq. (4) coincides with Eq. (2). In other cases, e.g., for bremsstrahlung in electron-electron collisions, the recoil is substantially different giving rise to strong suppression effects reminiscent of the LPM effect [43].

B. LPM effect

1. Radiation emission

The length over which a particle statistically scatters an angle $1/\gamma$ in an amorphous material due to multiple Coulomb scattering is given by

$$l_{\gamma}=\frac{\alpha}{4\pi}X_0 \tag{5}$$

where α is the fine-structure constant and X_0 the radiation length. Equation (5) is a conservative (only particles outside 2σ have scattered an angle $1/\gamma$) and approximate value in comparison with more accurate evaluations of the scattering angles, $\vartheta=13.6\ \mathrm{MeV}/\beta cp\times\sqrt{\Delta x/X_0}[1+0.038\ln(\Delta x/X_0)]$. Since the majority of radiation emission takes place within a cone of opening angle $1/\gamma$ to the direction of the electron, destructive interference may result if the electron scatters outside this zone. So if half the formation length exceeds the length l_{γ} [56], the emission probability decreases. Equation (4) combined with Eq. (5) leads to the threshold of the LPM effect at energies,

$$\hbar\omega^{\mathrm{q}}_{\mathrm{LPM}}=\frac{E^2}{E+E_{\mathrm{LPM}}} \quad \left(\hbar\omega^{\mathrm{c}}_{\mathrm{LPM}}\simeq\frac{E^2}{E_{\mathrm{LPM}}}\right) \tag{6}$$

where

$$E_{\mathrm{LPM}}=mc^2X_0/4\pi a_0=7.684\times X_0 \quad \mathrm{TeV/cm} \tag{7}$$

and a_0 is the Bohr radius. The value in parentheses denotes the classical (recoil-less) limit. As an example for Ir the value of E_{LPM} is 2247 GeV which means that $E=287$ GeV electrons yield threshold values of $\hbar\omega^{\mathrm{q}}_{\mathrm{LPM}}=32.4$ GeV and $\hbar\omega^{\mathrm{c}}_{\mathrm{LPM}}=36.7$ GeV in the quantum and classical cases, i.e., a quantum correction of 13%.

TABLE I. Theoretical values of $\hbar\omega^{\mathrm{q}}_{\mathrm{LPM}}$ in GeV.

	287	207	149
Iridium	32	17	9.3
Tantalum	24	13	6.8
Copper	7.2	3.8	2.0
Carbon	0.44	0.23	0.12

The LPM cross section for bremsstrahlung is given by Migdal as [2,3,19]

$$\frac{\mathrm{d}\sigma_{\mathrm{LPM}}}{\mathrm{d}\hbar\omega}=\frac{4\alpha r_e^2\xi(s)}{3\hbar\omega}\{y^2G(s)+2[1+(1-y)^2]\phi(s)\}\times Z^2\ln(184Z^{-1/3}) \tag{8}$$

where $G(s)$, $\phi(s)$ and $\xi(s)$ are functions of $s=\sqrt{E_{\mathrm{LPM}}\hbar\omega/8E(E-\hbar\omega)\xi(s)}$, i.e. $\xi(s)$ is defined recursively, but can be well approximated, see e.g., [19,44]. Here y denotes the fractional photon energy, $\hbar\omega/E$, Z the nuclear charge of the target and $r_e=\alpha^2a_0$ the classical electron radius. In the limit $G(s)=\phi(s)=1$ the Bethe-Heitler cross section is obtained. For a thorough treatment of the subject, see [19]. The Migdal expression, Eq. (8), has the advantage—from an experimentalist's point of view—of being relatively straightforward to implement in a Monte Carlo simulation (see below). As Klein [19] has put it: " . . . [the more recent] calculations are very complex and the descriptions frequently lack adequate information for independent computation . . . ."

The expected "threshold" energies, $\hbar\omega^{\mathrm{q}}_{\mathrm{LPM}}$, calculated from Eq. (6) for the targets Ir, Ta, Cu and C are given in Table I.

2. Pair-production

Since pair-production can be considered the crossing-symmetry equivalent of photon emission, this process can be expected to be suppressed by the LPM mechanism as well.

In the case of pair production, a classical analogue is the length it takes to separate a created pair transversely by two Compton wavelengths, λ_c, when the pair is emitted with an opening angle $1/\gamma_p$,

$$l_{\mathrm{f}}^{\mathrm{pair}}=2\gamma_p\lambda_c=\frac{2\gamma_p^2c}{\omega}. \tag{9}$$

Therefore, the formation length increases with the energy of the pair (where $\gamma_p\equiv\hbar\omega/mc^2$).

When calculated properly by means of longitudinal momentum transfer, the formation length for pair production becomes

$$l_{\mathrm{f}}^{\mathrm{pair}}=\frac{2\gamma_p^2c}{\omega^{\#}}\quad\text{with}\quad\omega^{\#}=\frac{\omega}{\xi_+\xi_-} \tag{10}$$

where $\xi_\pm$ is defined as $E_{\mathrm{e}^\pm}/\hbar\omega$ with $E_{\mathrm{e}^\pm}$ being the energy of the electron or positron. It is an important distinction relevant to the Landau-Pomeranchuk-Migdal effect that l_{f} increases with increasing energy of the pair, whereas the formation length for radiation emission decreases with increasing energy of the emitted photon for fixed energy of the radiating particle. On the other hand, the similarity between the two formation lengths when expressed as functions of γ, γ_p, ω^* and $\omega^{\#}$ reflects the symmetry of the processes. Thus, as the photon energy increases in the neighborhood of and beyond E_{LPM}, symmetric pairs, for which the formation length is longest, get suppressed first by the LPM mechanism. Therefore, an electromagnetic shower initiated by e.g., a photon with an energy far beyond E_{LPM} will develop in a manner quite different from ordinary showers because the photon emission tends to favor high photon energies and the pair production favors energetic electrons or positrons. For an example of LPM suppression in pair production, see e.g. [19].

C. Other suppression mechanisms

1. Thin target—Ternovskii-Shul'ga-Fomin effect

Since the formation length for radiation emission increases with decreasing photon frequency, at a certain point the formation zone extends beyond the thickness of the foil. In this case, the radiation yield also becomes suppressed. Studies of this effect were first performed by Ternovskii [45] and later extended by Shul'ga and Fomin [46–50], followed by Blankenbecler and Drell [51], and by Baier and Katkov [23]. The first confirmation was obtained in the SLAC experiments [20,48]. The phenomenon is also of substantial interest in QCD [52].

As to the extent of the effect, the analysis is applicable for target thicknesses $l_\gamma<\Delta x<l_{\mathrm{f}}$, see e.g. [50]. Therefore, by use of Eq. (4) and setting $\Delta x=l_{\mathrm{f}}/k_{\mathrm{f}}$ the effect appears for photon energies

$$\hbar\omega_{\mathrm{TSF}}=\frac{E}{1+\dfrac{k_{\mathrm{f}}\Delta x}{2\gamma\lambda_c}} \tag{11}$$

where $k_{\mathrm{f}}>1$. The threshold of the effect is located at $k_{\mathrm{f}}=1$, i.e. for $E/(1+\Delta x/2\gamma\lambda_c)$.

The magnitude of the effect is evaluated from the averaged radiation spectrum [50]

$$\left\langle\frac{\mathrm{d}E}{\mathrm{d}\omega}\right\rangle\simeq\frac{2\alpha}{\pi}\left[\ln\left(\frac{\Delta x}{l_\gamma}\right)-1\right] \tag{12}$$

and since for the Bethe-Heitler case $\langle\mathrm{d}E/\mathrm{d}\omega\rangle=4\Delta x/3X_0$, the suppression factor, κ, can conveniently be expressed as

$$\kappa\simeq\frac{k_\gamma}{6(\ln k_\gamma-1)} \tag{13}$$

where $\Delta x=k_\gamma l_\gamma$ and $k_\gamma>1$. As an example, for $\Delta x=4.4\%X_0$ and $E=287$ GeV, $k_\gamma=0.044\times4\pi/\alpha\simeq76$ yielding a suppression $\kappa=3.8$, but for photon energies lower than $\hbar\omega_{\mathrm{TSF}}=0.9$ GeV in Ir and 0.2 GeV in Cu, i.e. just below the observed photon energies in this experiment. The Ternovskii-

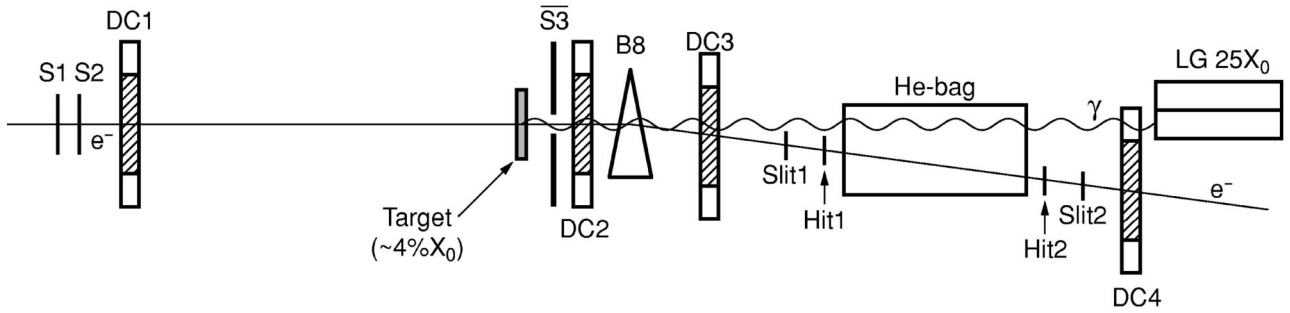

FIG. 2. A schematical drawing of the setup used in the CERN LPM experiment. Not to scale.

Shul'ga-Fomin effect may thus through pile-up have a marginal influence on the present data even though the threshold for observation is 2 GeV (see below).

2. Dielectric suppression—Ter-Mikaelian effect

In a medium with index of refraction, n, the velocity c/n replaces the photon velocity c. By use of this replacement in Eq. (1) and the index of refraction expressed as $n=1-\omega_p^2/2\omega^2$, a modified formation length is obtained

$$\frac{1}{l_{f\varepsilon}} \simeq \frac{\omega}{2\gamma^2 c} + \frac{\omega_p^2}{2\omega c} = \frac{1}{l_f} + \frac{1}{l_{df}} \tag{14}$$

where $\omega_p = \sqrt{4\pi NZe^2/m}$ is the plasma frequency, NZ being the electron density. The inverse of the dielectric formation length, $l_{df} = 2\omega c/\omega_p^2$, becomes dominating in Eq. (14) for photon energies below the value

$$\hbar\omega_d = \gamma\hbar\omega_p . \tag{15}$$

Therefore—in close analogy with the density effect in ionization energy loss—formation lengths beyond l_{df} are effectively cut off. Thus, for photon energies in the regime below $\hbar\omega_d$ the photon yield is suppressed by the Ter-Mikaelian effect, also known as dielectric suppression or the longitudinal density effect, see e.g. [41]. However, as plasma frequencies are of the order 50 eV/$\hbar$, even electron energies as high as 287 GeV in iridium lead to a suppression only below $\hbar\omega_d = 86$ MeV, i.e. practically irrelevant for this experiment.

III. EXPERIMENT

A. Setup

The experiment was performed in the H2 beam line of the CERN SPS in a tertiary beam of electrons with variable energy in the range 10–300 GeV, but with low intensity for very high and very low energies. The fraction of particles heavier than electrons in the beam is very low, estimated to about 10^{-3}. A schematical drawing of the setup is shown in Fig. 2. The incident electron beam is defined by three scintillator counters, S1, S2 and $\overline{S3}$ and the position and direction of each electron is found from its impact on drift chambers (DCs) both before, by DC1 and DC2, and after, by DC3 and/or DC4, a dipole magnet, B8. To minimize background, a vacuum tube with pressure $\simeq 10^{-6}$ mbar is used between DC1 and DC2. Each drift chamber has a sensitive region of 150×150 mm. In front of $\overline{S3}$ the target of about 4% X_0 is placed. The magnet and the position sensitive DCs enable energy tagging of the photons emitted in the target and the photons are finally intercepted in a lead glass (LG) detector. Each DC has a resolution of $\sigma\simeq100$ μm and the distances are such that the resulting angular resolution is about 10 μrad. For the tagging, DC3 is used for maximum acceptance while DC4 provides the optimum resolution for low energy photons.

B. Calibration

Calibration of the LG and the tagging system was performed by use of electron beams of nominal energies 10.0, 25.0, 50.0, 99.8, 149.1, 178.2, 206.7, 234.5, 261.2 and 286.6 GeV (referred to by their rounded values throughout) with B8 off and on ($Bl=4$ Tm). Consistency between the results from the tagging procedure and the lead glass calorimeter was confirmed as elaborated upon below. The lower energy threshold for the lead glass (LG) spectrum is 2 GeV while the relative resolution is $\sigma/E \simeq 0.16/\sqrt{E\ [\mathrm{GeV}]} + 0.0029 + 1.2\times10^{-4}E\ [\mathrm{GeV}]$ as found by directing the electron beam into the LG, see Fig. 3. The LG calorimeter was composed of 4 blocks (each being 25 radiation lengths long and 90×90 mm^2) arranged such that the beam was incident on the lower-right block. By scanning the beam across the main LG block it was assured that the beam hit this block centrally to within 5 mm. A small leakage to the adjacent 3 blocks was found and corrected for. Likewise, nonlinearity in the response of the LG calorimeter in its entirety was corrected for

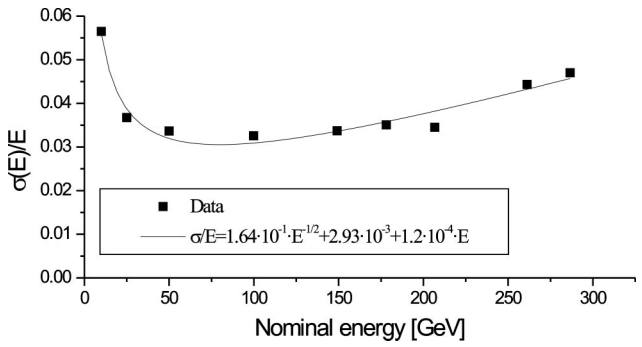

FIG. 3. The relative resolution of the lead glass calorimeter, $\sigma(E)/E$, as a function of electron energy.

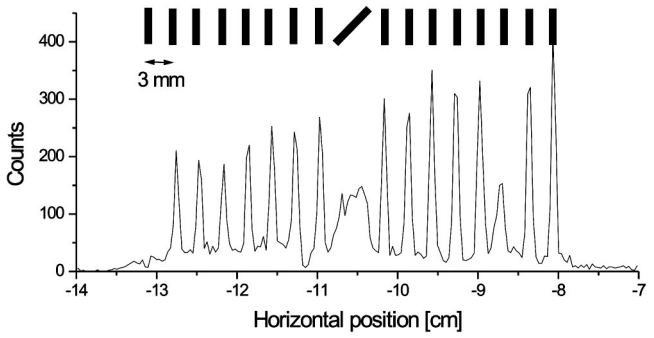

FIG. 4. Calibration data for drift chamber 4. The ''comb'' is due to slits in the veto (Slit1) combined with hits in the corresponding counter (Hit1) as indicated in the upper part of the figure.

in the analysis. After this correction, the deviation of the centroid of the calorimeter readout from the expected value was in all cases less than 3%, typically 1.5% and for energies below 50 GeV it was less than 1%.

In order to improve the resolution for low energy photons, the LG signal was fed to a passive splitter to produce two signals, one of which attenuated by a factor 10. The unattenuated signal, the so-called LGh, covered the range $\simeq 2$ to $\simeq 55$ GeV, while the attenuated LG covered the region from $\simeq 2$ GeV to substantially beyond the end point, E. For photon energies less than 20 GeV the LGh signal was used in the analysis and consistency between LGh and LG was confirmed in the region of overlap of the two signals.

For the tagging to function properly, the drift chambers must read the position accurately. From earlier experiments it is known that the DCs employed have a slightly nonlinear response due to a tiny acceleration of the drifting electrons across the cell. Therefore, the DCs were on-line calibrated by means of scintillator counters (Slit1, Hit1, Slit2 and Hit2) with known distance between slits cut in the scintillator material, see Fig. 4. The nonlinearities result in a maximum deviation of 0.25 mm which was taken into account in the analysis.

In order to correct for the background, an empty target run was performed for all three energies. The results of these runs, a background of about 0.7% X_0, have been subtracted from the data. In Fig. 5 is shown two of the background measurements with simulated values of 0.67% X_0 and 0.73% X_0 carbon targets for comparison. The background originates mainly from the aluminized mylar-windows of DC1 and DC2 and from the windows of the vacuum tubes.

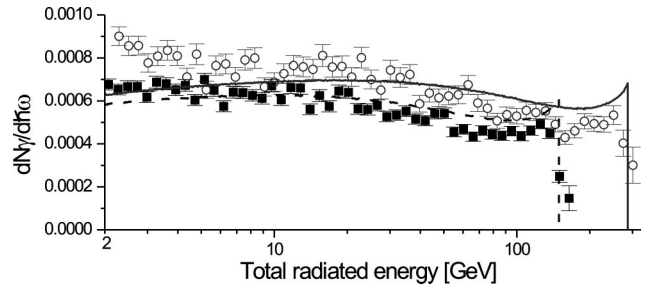

FIG. 5. Measured background spectra for the 149 (filled squares) and 287 GeV (open circles) runs. For comparison is shown the expected signal from a 0.67% X_0 C target at 149 GeV (dashed line) and a 0.73% X_0 C target at 287 GeV (full line).

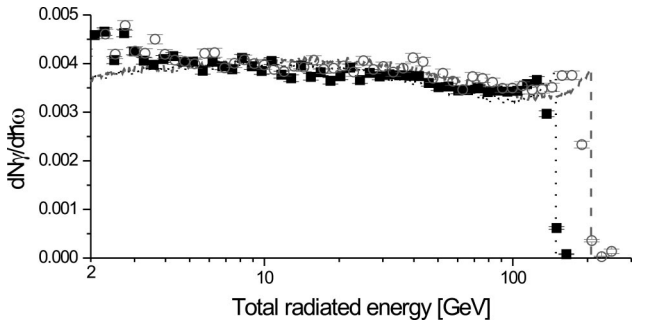

FIG. 6. Raw (not efficiency-corrected) data for 149 GeV (filled squares) and 207 GeV (open circles) electrons in carbon after subtraction of background. The lines represent simulated values for 149 GeV (dotted) and 207 GeV (dashed) based on the Bethe-Heitler limit of Eq. (8).

To calibrate the efficiency of the LG calorimeter as a function of photon energy, a carbon target—for which the LPM effect is absent in the detected range—was used. The result—with background duly subtracted—was compared to a simulation based on the standard Bethe-Heitler expression to extract the efficiency, see Fig. 6. The standard Bethe-Heitler spectrum was obtained by setting $E_{\mathrm{LPM}}=10^9$ GeV. No attempt to reproduce the observed background by detailed simulation was performed. The correction arising from the efficiency was for all photon energies small, typically 4–5 %. The efficiency arises due to a number of geometrical factors, for instance pair production in the He-bag where the opening angle of the pair is such that it misses the LG or an excess of counts due to interaction of the spent electron with the He-bag vessel that may be partly intercepted by the LG. The characteristic frequency of synchrotron radiation for 287 GeV electrons in a 2T field (about max. value in B8) is $\hbar\omega_c \simeq 0.1$ GeV beyond which the spectrum falls off roughly exponentially and the total energy loss amounts to 0.7 GeV. The small ''bump'' at very low photon energies in Fig. 6 can thus not be explained by synchrotron radiation. The simulations were performed by the use of GEANT with an implementation of the cross section from Eq. (8).

C. Targets

The absolute value of the nominal radiation length of each of the targets was determined by weighing and measuring the foils to obtain the areal density and using Tsai's tabulated values for the unit radiation length [53]. The resulting values are $\Delta t_{\mathrm{C}}/X_0 = 4.14 \pm 0.05\%$, $\Delta t_{\mathrm{Cu}}/X_0 = 4.40 \pm 0.03\%$, $\Delta t_{\mathrm{Ta}}/X_0 = 4.45 \pm 0.05\%$ and $\Delta t_{\mathrm{Ir}}/X_0 = 4.36 \pm 0.10\%$ for C, Cu, Ta and Ir, respectively, in good agreement with the values specified by the supplier. The carbon target was specified to be 99.5% pure (main contaminants iron oxide, silica and aluminum), while the remaining targets were 99.9% pure.

In order to reduce the influence of pile-up of several sequentially emitted photons a target thickness of $\simeq 4\%$ X_0 was chosen. This means that the average photon multiplicity above the threshold of 2 GeV in 0.128 mm Ir is $\simeq 1.1\%$, i.e.

the probability of two-photon emission is low. The simulations show, however, that even in a target as thin as 4% X_0 the contribution from pile-up is affecting the spectrum visibly, up to 20%.

Furthermore, as pile-up may mimic the suppression effect caused by the LPM mechanism (see e.g., [24]), we chose targets of almost equivalent thickness in units of radiation lengths. Since the LPM effect is proportional to X_0 while the pile-up depends on the thickness *in units of* X_0, a comparison between the targets reveals the LPM effect, irrespective of pile-up.

The measurement sequence—which is relevant for an evaluation of systematic errors in the comparison between targets and energies—was as follows: calibration, then first all targets at 287 GeV, starting with Ir, C, empty target, Ta and then Cu, followed by the same sequence of targets at 207 GeV, recalibration and finally 149 GeV again with the same sequence of targets. No significant change in beam-angle and/or -position was observed from one target or energy to the next. Any small change was compensated by off-line selections of events during analysis.

1. Contribution from target electrons and the Coulomb correction

According to Tsai [53] the unsuppressed bremsstrahlung cross section equals

$$\frac{\mathrm{d}\sigma}{\mathrm{d}\hbar\omega} = \frac{4\alpha r_e^2}{\hbar\omega}\left[\left(\frac{4}{3}-\frac{4}{3}y+y^2\right)[Z^2(L_{\mathrm{rad}}-f)+ZL'_{\mathrm{rad}}] + \frac{1}{9}(1-y)(Z^2+Z)\right] \tag{16}$$

where (for $Z \geqslant 5$) $L_{\mathrm{rad}} = \ln(184Z^{-1/3})$ is the radiation logarithm for interaction with the nuclear field ($\propto Z^2$), f is the Coulomb correction and $L'_{\mathrm{rad}} = \ln(1194Z^{-2/3})$ is the radiation logarithm for interaction with the target electrons ($\propto Z$). Equation (16) applies in the limit of complete screening, i.e. for electrons of sufficiently high energy and excluding photon emission energies close to that of the incident electron. As we are considering ultrarelativistic electrons ($\gamma \simeq 5 \times 10^5$) and the region of main interest is low photon energies, the requirement of complete screening is fulfilled.

The tabulated values of the radiation length used for our target thickness evaluations are inversely proportional to Eq. (16) if the term $c(y) = (1-y)(Z^2+Z)/9$ is ignored [53]. This correction term is 2.4% of the terms retained in the case of Ir and 1.7% in the case of C for soft photons ($y \leqslant 0.2$) and tends to zero for hard photons. We note that Eq. (8) transforms into Eq. (16) in the limit $G(s) = \phi(s) = 1$ when $c(y)$ is neglected, by the substitution $Z^2 L_{\mathrm{rad}} \rightarrow Z^2(L_{\mathrm{rad}}-f)+ZL'_{\mathrm{rad}}$, corresponding to a redefinition of the radiation length. This redefinition is possible since the energy behavior of terms proportional to Z and Z^2 is equal in the complete screening case. Disregarding the small correction $c(y)$, the contribution from target electrons (and the Coulomb correction f which amounts to 8% for Ir) is thus taken into account by scaling, through the usage of Tsai's tabulated values for X_0.

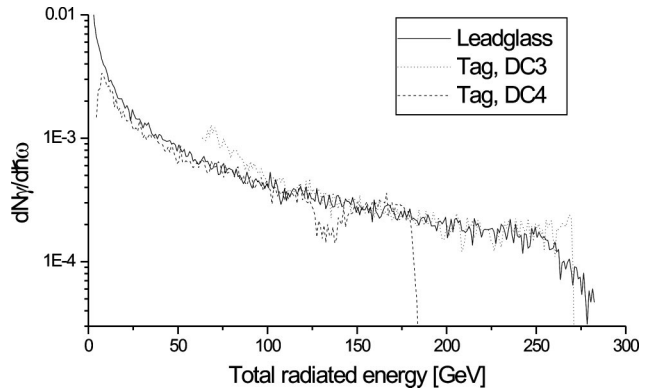

FIG. 7. Counting spectra, $\mathrm{d}N/\mathrm{d}\hbar\omega$, as a function of photon energy, $\hbar\omega$, linearly binned and plotted on a logarithmic vertical scale. The dotted line denotes the tagging in DC3, the dashed line denotes the tagging in DC4 while the full line represents the data obtained by the lead glass calorimeter. All three sets are for 287 GeV electrons on 0.128 mm Ir (4.36% X_0). Background has been subtracted from the data sets but corrections for efficiencies have not been included. Data points where the relative uncertainty exceeds 25% have been discarded.

Since the kinematics of scattering off electrons or nuclei are different, it is possible that the term proportional to Z remains unsuppressed for energies where the term proportional to Z^2 is suppressed. Simulations where both terms are suppressed and with suppression of only the nuclear term show that the difference between these descriptions is small (see below).

D. Analysis

1. Angular resolution

The drift chambers used for the present experiment, once properly calibrated, provide a spatial resolution of approximately $\sigma = 100$ μm. With distances of 61.42 m between DC1 and DC2 and 18.91 m between DC2 and DC4 this gives an extremely good angular resolution on the entry as well as on the exit side of the target foil. Since two chambers are needed to determine an angle, the uncertainty in deflection angle by DC1, DC2 and DC4 is $\Delta\theta_{\mathrm{DC}} \simeq \sqrt{2} \times 100$ μm$(1/61\ \mathrm{m} + 1/19\ \mathrm{m}) \simeq 10$ μrad. This can be verified from the data by applying tight cuts on DC1 and DC2 and observing the width in DC4 which should be $\simeq 10$ μrad $\times 18$ m $= 0.18$ mm for the empty target run. By extrapolation to zero of the width of the cuts, the experimental value is 0.19 mm, yielding confidence in e.g., angular selections (see below).

2. Tagging spectrometer

In Fig. 7 is shown the results obtained for the iridium target with 287 GeV electrons by use of the lead glass calorimeter and the tagging procedure. Clearly, the overall agreement is good in the sections of overlapping sensitive regions.

For drift chamber 3, the direct (B8 = 0 A) electron beam crossed the sensitive region with the center at a distance of 10 mm from the edge. The distance from DC3 to the center

of B8 was 1.77 m. Thus, operation with B8 at the standard value of integrated field 4.052 Tm provided a sensitivity to photons in the range from $\simeq 0$ GeV to $\simeq 271$ GeV for electrons of 287 GeV.

For drift chamber 4, the direct electron beam was kept outside the sensitive region with the center at a distance of 45 mm from the edge. The distance from DC4 to the center of B8 was 17.23 m providing a sensitivity to photons in the range from $\simeq 0$ GeV to $\simeq 180$ GeV for electrons of 287 GeV. For DC3 as well as DC4, these upper thresholds of sensitivity to photons are in excellent agreement with the upper cutoffs observed in Fig. 7. The dip in efficiency observed for photon energies near 130 GeV for tagging in DC4 is correlated with hits in the DC near the anode-wire where the efficiency is low due to a poorer development of the electron avalanche in the chamber.

It is easy to show that the relative energy resolution is given by

$$\frac{\mathrm{d}E_\gamma}{E_\gamma} = \frac{\mathrm{d}\theta}{\theta}\left(\frac{E_e}{E_\gamma} - 1\right) \tag{17}$$

where θ is the deflection angle and E_γ is the energy of the radiated photon. When the magnet B8 is operated at 4.052 Tm (yielding a deflection of 4.2 mrad at 287 GeV) and with a combined angular resolution of two DCs of $\mathrm{d}\theta \simeq 10$ μrad as expected for DC2-DC4, we get a relative resolution of 10% at a photon energy of 7 GeV. For DC3 which is a factor 6 closer to DC2, the angular resolution is substantially worse such that photon energies below at least $\simeq 40$ GeV should be disregarded. As seen in Fig. 7 an excess of counts compared to the LG is observed in the DC3 tagging for energies below $\simeq 100$ GeV. This is a consequence of a wrong evaluation of the photon energy due to the finite resolution and is compensated at even lower photon energies (not shown) where however, the resolution becomes very poor, resulting in a substantial scatter of data points. The comparison between the tagging and lead glass procedures therefore yields very satisfactory results in the regions to be expected amenable to analysis. Especially reassuring is the very good agreement in absolute scale.

IV. RESULTS AND DISCUSSION

A. Total spectra

The counting spectra (logarithmic binning, 25 bins/decade) obtained for 149, 207 and 287 GeV electrons impinging on Ir, Ta and Cu targets, respectively, are shown in Figs. 8–11. The dotted lines denote the values obtained by a Monte Carlo simulation based on a Bethe-Heitler bremsstrahlung spectrum for the nominal thickness in units of X_0, i.e., including the effect of pile-up, but excluding any suppression effects. The full lines denote the values obtained by the simulation based on the LPM corrected bremsstrahlung spectrum. The simulations are performed using a lower energy threshold of 0.1 GeV and 600 channels from 1 GeV to the end point energy. Rescaling of the relative bin-size has been performed to enable comparison, but no scaling of e.g., target thickness has been done.

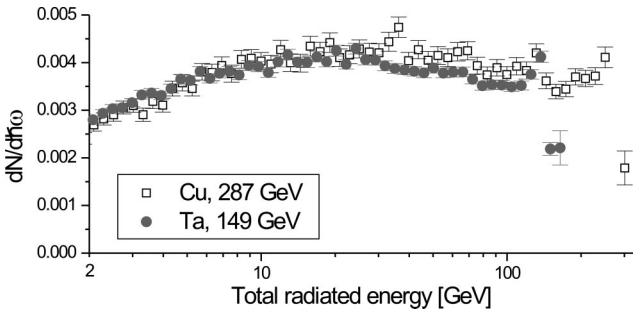

FIG. 8. Counting spectra, $\mathrm{d}N/\mathrm{d}\hbar\omega$, as a function of photon energy, $\hbar\omega$, logarithmically binned and plotted on a logarithmic scale. The filled circles are for 149 GeV electrons in 4.45 ± 0.05 X_0 Ta and the open squares for 287 GeV electrons in 4.40 ± 0.03 X_0 Cu.

As expected from Table I and seen in Fig. 8, the measured spectrum for copper at 287 GeV is very similar to that of tantalum at 149 GeV for low photon energies. This is a strong experimental indication that the ''threshold'' value as e.g., calculated from Eq. (6) is decisive for the suppression

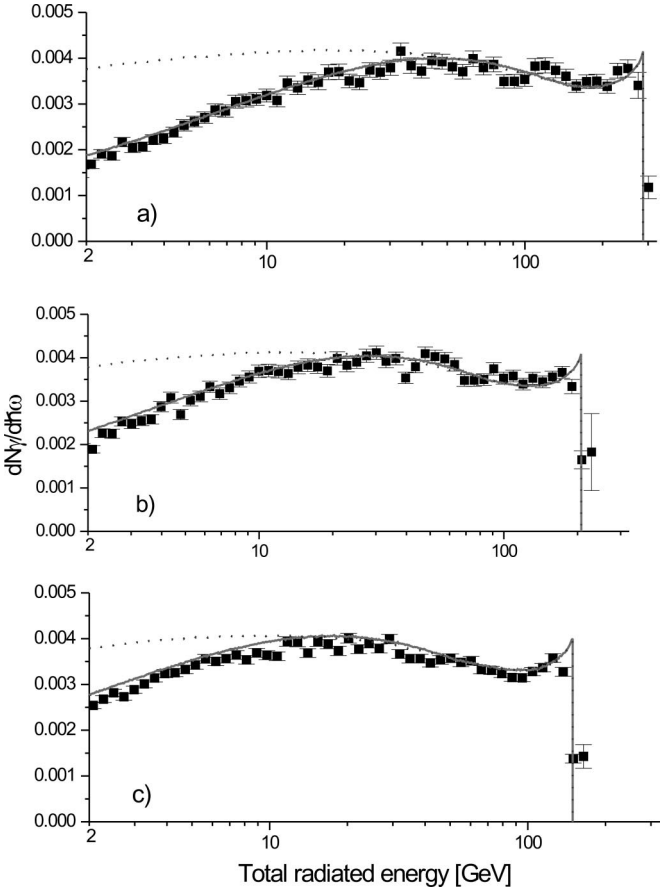

FIG. 9. Bremsstrahlung spectrum, $\mathrm{d}N_\gamma/\mathrm{d}\hbar\omega$, for (a) 287 GeV, (b) 207 GeV and (c) 149 GeV electrons on 0.128 mm Ir (4.36% X_0). The total radiated energy, $\hbar\omega$, is presented in logarithmic bins (25 per decade) and plotted on a logarithmic scale. The vertical scale is normalized to the number of incoming electrons. The dotted line is the result of a simulation based on a pure Bethe-Heitler spectrum while the full line includes the LPM suppression.

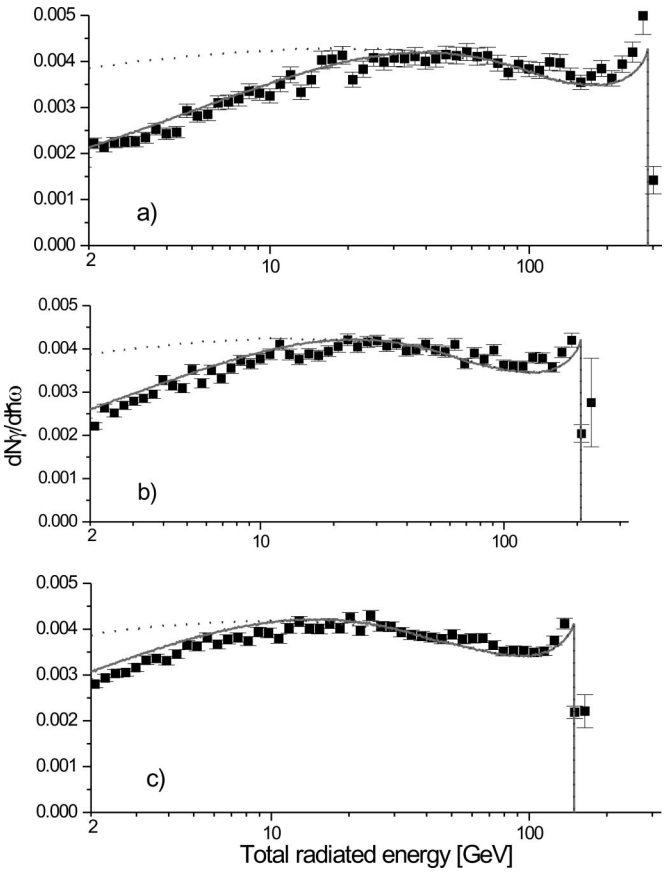

FIG. 10. As Fig. 9, but for tantalum.

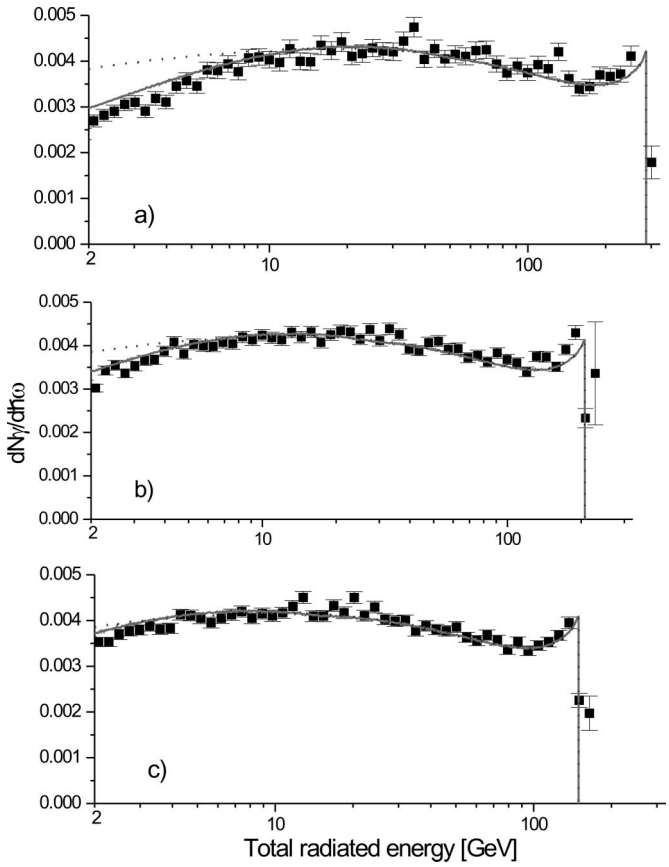

FIG. 11. As Fig. 9, but for copper.

mechanism, irrespective of the type of material (apart from this particular combination of nominal radiation length and energy).

In Fig. 9 the results for the three energies in Ir are shown. A comparison between experimental values, the LPM suppressed spectrum and the unsuppressed Bethe-Heitler type spectrum clearly shows the strong suppression and its increase with increasing beam energy. The overall agreement between the experiment and the LPM spectrum is very satisfactory, although at low photon energies the scale of the experimental values seems about 5% too low. The slight discrepancy at the highest photon energies where the cross section (which is strictly valid only for $\gamma \rightarrow \infty$) has a local maximum, is due to the finite resolution of the lead glass which ''smears'' the peak. The first part of this peak is seen more clearly in the tagging spectrum, see Fig. 7, which, however, is cut off at a photon energy in the neighborhood of 271 GeV.

In Fig. 10 the results for the three energies in Ta are shown. In this case the agreement is not quite as convincing as for Ir, indicating a slightly stronger suppression than expected. This also bears out in the experimental value for E_{LPM}, see below.

Finally, for Cu shown in Fig. 11, the overall agreement is good although the scatter of the experimental values is somewhat more pronounced. The overall picture shows that the LPM suppression is pronounced at low photon energies and it is evident that the effect is very strong for the dense, high-Z targets chosen, while Cu has a significantly smaller suppression which appears at lower photon energies. Furthermore, the agreement is good over the entire spectrum for all three energies and all targets, although there is a tendency for the data to lie below the simulation for lower electron energies.

B. Reduced multiple scattering

Since the LPM effect is a result of multiple scattering within the formation zone, it should be possible by restricting the range of scattering angles to influence the threshold of the LPM effect. As the opening angle of the photon emission or pair creation is of the order $1/\gamma = mc/p \ll 13.6\ \mathrm{MeV}/(\beta cp)$ with a typical distance $\simeq X_0$ between emissions, the multiple scattering is dominating for all energies. In fact, since $\vartheta \propto \sqrt{\Delta x/X_0}$ a restriction of scattering angles by e.g., $\vartheta' = k_\vartheta \cdot \vartheta$ where $0 \leqslant k_\vartheta \leqslant 1$ yields a change in the effective LPM threshold to $E'_{\mathrm{LPM}} = E_{\mathrm{LPM}}/k_\vartheta^2$. Clearly, due to the connection between angle, momentum and scattering in the horizontal plane such a selection can only be performed in the vertical plane where the momentum (due to the lack of vertical dispersion after B8) does not enter as a variable. As the angular resolution is about 10 μrad, but in one plane only, and the scattering angle is well approximated by $\vartheta_{\Delta x} = 13.6\ \mathrm{MeV}/(\beta cp)\sqrt{\Delta x/X_0}$ with $\Delta x/X_0 \simeq 4.4\%$ which gives 14 μrad for 207 GeV in Ir, the angular resolution is just at the limit of enabling evidence for a potentially reduced LPM effect.

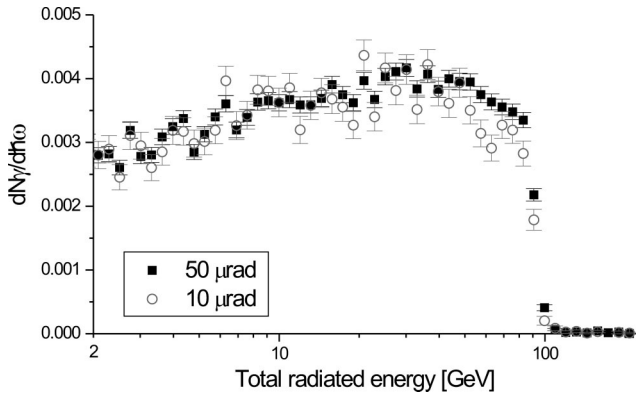

FIG. 12. Counting spectra, $dN/d\hbar\omega$, as a function of photon energy, $\hbar\omega$, logarithmically binned and plotted on a logarithmic scale. The data points are for 207 GeV electrons on 0.128 mm Ir (4.36% X_0) with background subtracted. The open circles are obtained with a cut $\Delta\theta_y \leqslant 10$ μrad in vertical deflection angle and the filled squares for $\Delta\theta_y \leqslant 50$ μrad. The upper limit of photon energies at $\hbar\omega \simeq 100$ GeV reflects the acceptance of DC4.

The results of two angular selections performed on the 207 GeV iridium data are shown in Fig. 12. No clear change of the suppression can be observed.

In the search for EeV-ZeV electromagnetically initiated extended air showers, the effective area of the detector represents a subsection of the actual extent of the air shower and therefore a potential change in the effective value of the LPM threshold.

C. Determination of E_{LPM}

To compare the experimental data with the predictions based on the theoretical model outlined above and Monte Carlo simulations, the LPM effect had to be included in the GEANT code by modifying the subroutines which calculate the differential and total bremsstrahlung cross section. Equation (8) above [together with the approximations given in Eqs. (73)–(77) of [19]] was used for the former. For the total cross section, in order to reduce the influence of the $1/\hbar\omega$ factor in Eq. (8), it proved very convenient to integrate numerically the difference between Eq. (8) and the standard Bethe-Heitler expression and to add the integral of the latter obtained analytically.

In order to determine an experimental value of E_{LPM} we followed a minimum chi-square procedure whereby, for every target and beam energy, a set of Monte Carlo simulations for different values of this parameter were performed determining analytically, for each of the resulting histograms, the overall normalization factor which best fitted the corresponding experimental histogram. The energy resolution of the calorimeter was taken into account in the simulations; as expected it only affected the contents of a few bins around the highest and lowest energies; they were excluded from the analysis which included only bin energies above 2 GeV. Another reason for excluding the lowest energy bins is their sensitivity to the threshold energy of radiated photons adopted in the simulations. A value of 0.1 GeV was used for the threshold but values up to 1 GeV were investigated to examine its influence on the spectra which turned out to be negligible. A parabola was fitted to the points in the χ^2-E_{LPM} plane to find the best value of E_{LPM} together with its standard deviation. In most cases a minimum value of χ^2 within one standard deviation from the expectation value was obtained and in no case did the deviation exceed two standard deviations.

TABLE II. Reduced χ^2-values for the data for each energy (in GeV) and each target including only statistical uncertainties, compared to the simulation based on the theoretical values of E_{LPM}. The number of degrees of freedom was 50, 47 and 44, respectively.

	287	207	149
Iridium	1.0	1.6	1.2
Tantalum	1.3	3.0	3.8
Copper	2.1	2.7	

In Table II we present the values of the reduced χ^2. For Ir, the agreement is good for all three energies, for Cu it is substantially worse, while for Ta the agreement is good for 287 GeV while being clearly poorer for lower energies.

The values found by the χ^2 procedure are given in Table III, including an evaluation of the systematic uncertainties. Since the lower energy threshold coincides with $\hbar\omega^{\mathrm{q}}_{\mathrm{LPM}}$ for Cu at 149 GeV, the value of E_{LPM} cannot be extracted in this case.

As discussed above, the kinematics of scattering off electrons or nuclei are different, and it is possible that the term proportional to Z remains unsuppressed for energies where the term proportional to Z^2 is suppressed. A comparison of simulations where both terms are suppressed and with suppression of only the nuclear term yields changes that lie within about half the RMS statistical uncertainty and does not improve the χ^2-value.

1. Systematic uncertainties

As seen from the values in the table and from Fig. 13, the experimental values tend to lie substantially below the theoretical one when only the statistical uncertainties are consid-

TABLE III. Experimental and theoretical values of E_{LPM} in TeV for each energy (in GeV) and each target. Both statistical and estimated systematic uncertainties are given.

	287	207	149	Theory, Eq. (7)
Iridium	$2.2\pm0.1\pm0.2$	$1.9\pm0.1\pm0.3$	$2.1\pm0.1\pm0.3$	2.247
Tantalum	$2.5\pm0.2\pm0.3$	$2.3\pm0.1\pm0.4$	$2.1\pm0.1\pm0.5$	3.143
Copper	$7.4\pm0.5\pm2$	$7.5\pm0.4\pm2$		11.06

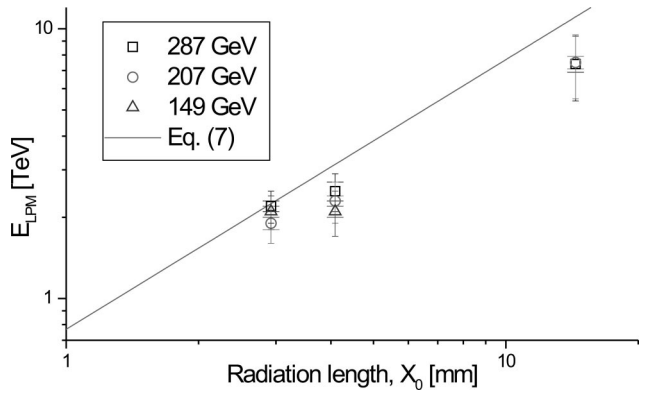

FIG. 13. Experimental and theoretical values of E_{LPM} as a function of nominal radiation length. Both statistical (wide error bars) and estimated systematic uncertainties (narrow error bars) are shown.

ered. The overall scale does not affect this conclusion drastically. One explanation could be systematic effects which e.g., yield too high values for the carbon spectrum, in particular for low photon energies, see Fig. 6. Since the experimental efficiency is derived from this, a slightly insufficient account for background counts may result in an efficiency that could affect the spectrum on a 5% scale (which would result in a wrong evaluation of E_{LPM} by about 12% for Ir). The systematic errors include the targets thicknesses ($\simeq 1\%$), photon energy calibration [$\simeq 2\%$, but energy dependent, to a small extent influenced by the accuracy with which the input energy is known (about 1% [55])], background subtraction ($\simeq 2\%$), simulation ($\simeq 1\%$) and efficiency correction ($\simeq 4\%$, also energy dependent), resulting in a total systematic uncertainty of about 5% which depends on photon energy.

We emphasize that the χ^2-analysis is very sensitive to small changes in the spectrum, in particular at low energies. Thus, in view of the systematic uncertainties we do not attempt to claim an observation of a failure of the theoretical assessment of E_{LPM}, as from the analysis we cannot exclude e.g. an insufficient account of background events on the few percent level. In any case, the good agreement between measured and nominal spectra shown in Figs. 9–11 is visible over the entire energy range, in particular for Ir. This agreement supports the validity of Migdal's theory, also in the quantum regime.

From the experimental point of view, the discrepancy for e.g., Ta at 149 GeV can be remedied by an ''artificial'' efficiency that increases logarithmically with photon energy from 0.92 to 1.04, i.e., $\varepsilon(E)=0.029\ln(E[\mathrm{GeV}])+0.9$. This correction is slightly large compared to the estimated systematic uncertainty, which is also reflected in Ta data point error bars being slightly low in Fig. 13. We emphasize that attempts to derive such ''artificial'' efficiencies will only remedy one target (e.g., Ta) while for other targets (as Ir) the agreement becomes poorer when the same correction is applied.

Ignoring the term $c(y)=(1-y)(Z^2+Z)/9$ in Eq. (16) makes a small correction at low photon energies (1.7% correction for carbon and 2.4% for Ir) which, however, would only make a minute impact on the evaluation of E_{LPM}.

On the theoretical side, the application of the Migdal expression, Eq. (8), is slightly doubtful when it comes to corrections on the few percent scale. Other, more recent theories of e.g., Baier and Katkov [23–25], include Coulomb corrections directly in the expression for the spectral distribution of the radiation probability [23] as well as a correction term derived from an expansion of the electron propagator. This correction term is energy dependent and not insignificant for 250 GeV electrons penetrating gold [25], peaking near $y \simeq 0.1$, i.e., in the main region of interest here. It increases the theoretically expected values near and below $\hbar\omega^{\mathrm{q}}_{\mathrm{LPM}}$ and thus makes the agreement between theory and data slightly poorer in all cases. We emphasize that no renormalization of the target thicknesses has been performed, in contrast to the SLAC measurements.

If an average of the experimentally determined values of E_{LPM} is used to extract the coefficient of proportionality from Eq. (7) the result is $E_{\mathrm{LPM}}=5.3\pm 0.3\pm 1.5X_0\times\mathrm{TeV/cm}$ with statistical and estimated systematic errors, respectively.

D. Suppression and possible compensation

As discussed in [1], by integration of each of the two intervals split by $\hbar\omega^{\mathrm{q}}_{\mathrm{LPM}}$ we get suppression factors, η_{low} and η_{high} (integral of the Bethe-Heitler simulated spectrum divided by the data). As seen from Table IV the latter is clearly consistent with 1 while the former indicates a strong suppression. Furthermore, the same procedure applied to the upper 10 or 20% of the spectrum, $\eta_{10/20}$, shows no sign of a compensating effect. Inclusion of a 5% systematic uncertainty does not alter this conclusion.

The possible compensation effect that could counteract the LPM suppression discussed by Bell [54] is thus not observed in the presented data.

V. CONCLUSION

We have presented measurements of the LPM suppression in the energy regime where quantum effects such as recoil become significant. Comparison with simulated theoretical spectra based on the theory of Migdal shows good agreement

TABLE IV. The suppression factors for Ir; see text for details.

Energy	η_{total}	η_{low}	η_{high}	η_{20}	η_{10}
287 GeV	1.02 ± 0.09	1.27 ± 0.10	0.99 ± 0.08	1.00 ± 0.06	1.04 ± 0.06
207 GeV	1.02 ± 0.13	1.22 ± 0.09	1.00 ± 0.12	1.06 ± 0.11	1.10 ± 0.12
149 GeV	1.06 ± 0.07	1.20 ± 0.05	1.06 ± 0.07	1.14 ± 0.06	1.21 ± 0.07

for the targets Ir, Ta and Cu for electron energies 149, 207 and 287 GeV. The theoretical reproduction of experimental values yields confidence in extrapolations of the theories to energies and densities where quantum effects are dominating as e.g. for calorimetry of secondary leptons at the future LHC or in ZeV air showers. A comparison between simulations with the ''threshold'' energy, E_{LPM}, as a free parameter and the data is also shown. This analysis reproduces the expected trend as a function of nominal radiation length, but yields values that are slightly low compared to Migdal's theory. Finally, we show experimentally that the parameter, E_{LPM}, is decisive for the onset of suppression.

ACKNOWLEDGMENTS

U.I.U. wishes to thank Professor M. L. Ter-Mikaelian for his keen interest and encouragement during discussions related to the presented experiment. U.I.U. acknowledges support from the ICE center, funded by the Danish Natural Science Research Council.

[1] H.D. Hansen *et al.*, Phys. Rev. Lett. **91**, 014801 (2003).
[2] A.B. Migdal, J. Exp. Theor. Phys. **32**, 633 (1957); Phys. Rev. **103**, 1811 (1956).
[3] L. Landau and I. Pomeranchuk, Dokl. Akad. Nauk SSSR **92**, 735 (1953); [English translation: L. Landau, *The Collected Papers of L.D. Landau* (Pergamon, New York, 1965), p. 589].
[4] X. Bertou, P. Billoir, and S. Dagoret-Campagne, Astropart. Phys. **14**, 121 (2000).
[5] M. Takeda *et al.*, Phys. Rev. Lett. **81**, 1163 (1998).
[6] T. Stanev and H.P. Vankov, Phys. Rev. D **55**, 1365 (1997).
[7] A.N. Cillis, H. Fanchiotti, C.A. Garcia Canal, and S.J. Sciutto, Phys. Rev. D **59**, 113012 (1999).
[8] S.R. Klein *et al.*, in *Lepton and Photon Interactions*, edited by P. Drell and D. Rubin, AIP Conf. Proc. No. **302** (AIP, New York, 1994).
[9] S.R. Klein, in *Workshop on Observing Giant Cosmic Ray Air Showers from* $>10^{20}$ eV *Particles from Space*, edited by J. F. Krizmanic, Jonathan F. Ormes, and Robert E. Streitmatter, AIP Conf. Proc. No. **433** (AIP, Woodbury, NY, 1998).
[10] H.P. Vankov, N. Inoue, and K. Shinozaki, Phys. Rev. D **67**, 043002 (2003).
[11] A.H. Sørensen, Z. Phys. C **53**, 595 (1992).
[12] R. Baier, Yu.L. Dokshitzer, S. Peigne, and D. Schiff, Phys. Lett. B **345**, 277 (1995).
[13] M. Gyulassy and X.-N. Wang, Nucl. Phys. **B420**, 583 (1994).
[14] X.-N. Wang, M. Gyulassy, and M. Plümer, Phys. Rev. D **51**, 3436 (1995).
[15] B. Kämpfer and O.P. Pavlenko, Phys. Lett. B **477**, 171 (2000).
[16] X. Guo and X.-N. Wang, Phys. Rev. Lett. **85**, 3591 (2000).
[17] X.-N. Wang, X. Guo, Nucl. Phys. **A696**, 788 (2001).
[18] A. Sedrakian and A.E.L. Dieperink, Phys. Rev. D **62**, 083002 (2000).
[19] S. Klein, Rev. Mod. Phys. **71**, 1501 (1999).
[20] P.L. Anthony *et al.*, Phys. Rev. Lett. **75**, 1949 (1995).
[21] P.L. Anthony *et al.*, Phys. Rev. Lett. **76**, 3550 (1996).
[22] P.L. Anthony *et al.*, Phys. Rev. D **56**, 1373 (1997).
[23] V.N. Baier and V.M. Katkov, Phys. Rev. D **57**, 3146 (1998).
[24] V.N. Baier and V.M. Katkov, Phys. Rev. D **59**, 056003 (1999).
[25] V.N. Baier and V.M. Katkov, Phys. Rev. D **62**, 036008 (2000).
[26] A.V. Koshelkin, JETP **91**, 265 (2000).
[27] B.G. Zakharov, Phys. At. Nucl. **62**, 1008 (1999).
[28] B.G. Zakharov, JETP Lett. **64**, 781 (1996).
[29] B.G. Zakharov, JETP Lett. **63**, 952 (1996).
[30] R. Blankenbecler, Phys. Rev. D **55**, 190 (1997).
[31] V.N. Baier and V.M. Katkov, Phys. Rev. D **60**, 076001 (1999).
[32] V.N. Baier and V.M. Katkov, Phys. Rev. D **63**, 116008 (2001).
[33] P. Arnold, G.D. Moore, and L.G. Yaffe, J. High Energy Phys. **06**, 030 (2002).
[34] P. Aurenche, F. Gelis, and H. Zaraket, Phys. Rev. D **62**, 096012 (2000).
[35] B.G. Zakharov, Phys. At. Nucl. **61**, 838 (1998).
[36] B.G. Zakharov, JETP Lett. **73**, 49 (2001).
[37] R. Baier *et al.*, Phys. Lett. B **345**, 277 (1995); Nucl. Phys. **B478**, 577 (1996).
[38] U.A. Wiedemann and M. Gyulassy, Nucl. Phys. **B560**, 345 (1999).
[39] M.L. Ter-Mikaelian, private communication.
[40] K. Kirsebom *et al.*, Nucl. Instrum. Methods Phys. Res. B **174**, 274 (2001).
[41] M.L. Ter-Mikaelian, *High-Energy Electromagnetic Processes in Condensed Media* (Wiley Interscience, New York, 1972).
[42] U. Mikkelsen, Ph.D. thesis, Aarhus University 1997, CERN-THESIS 97-009, unpublished.
[43] V.N. Baier and V.M. Katkov, Phys. Rev. D **66**, 053009 (2002).
[44] T. Stanev Phys. Rev. D **25**, 1291 (1982).
[45] F.F. Ternovskii, JETP **12**, 123 (1961).
[46] N.F. Shul'ga and S.P. Fomin, JETP **27**, 117 (1978).
[47] N.F. Shul'ga and S.P. Fomin, Phys. Lett. **114A**, 148 (1986).
[48] N.F. Shul'ga and S.P. Fomin, JETP Lett. **63**, 873 (1996).
[49] N.F. Shul'ga and S.P. Fomin, Nucl. Instrum. Methods Phys. Res. B **145**, 73 (1998).
[50] N.F. Shul'ga and S.P. Fomin, JETP **86**, 32 (1998).
[51] R. Blankenbecler and S.D. Drell, Phys. Rev. D **53**, 6265 (1996).
[52] B.Z. Kopeliovich, A. Schäfer, and A.V. Tarasov, Phys. Rev. C **59**, 1609 (1999).
[53] Y. Tsai, Rev. Mod. Phys. **46**, 815 (1974).
[54] J.S. Bell, Nucl. Phys. **8**, 613 (1958).
[55] N. Doble and W. Herr (private communication).
[56] This half is a somewhat arbitrarily chosen number which results in differing definitions of E_{LPM}—one could also have chosen the length $l_\gamma = \alpha/2\pi \cdot X_0$, reflecting the scatter of particles outside 1σ. Here we choose the convention of [19] for E_{LPM}.